This article was downloaded by:
On: *31 January 2011*
Access details: *Access Details: Free Access*
Publisher *Taylor & Francis*
Informa Ltd Registered in England and Wales Registered Number: 1072954 Registered office: Mortimer House, 37-41 Mortimer Street, London W1T 3JH, UK

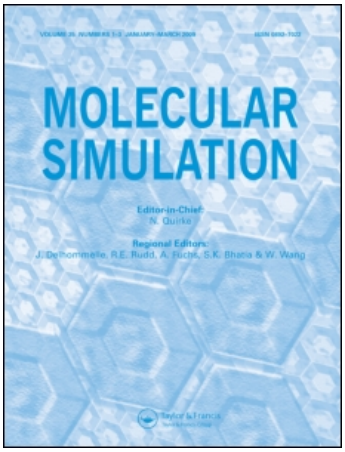

Molecular Simulation
Publication details, including instructions for authors and subscription information:
http://www.informaworld.com/smpp/title~content=t713644482

A molecular dynamics study of nano-bubble surface tension

H. Rezaei Nejad[a]; M. Ghassemi[a]; S.M. Mirnouri Langroudi[a]; A. Shahabi[a]
[a] Mechanical Engineering Department, K.N. Toosi University of Technology, Tehran, Iran

Online publication date: 28 January 2011

To cite this Article Rezaei Nejad, H. , Ghassemi, M. , Mirnouri Langroudi, S.M. and Shahabi, A.(2011) 'A molecular dynamics study of nano-bubble surface tension', Molecular Simulation, 37: 1, 23 — 30
To link to this Article: DOI: 10.1080/08927022.2010.513007
URL: http://dx.doi.org/10.1080/08927022.2010.513007

PLEASE SCROLL DOWN FOR ARTICLE

Full terms and conditions of use: http://www.informaworld.com/terms-and-conditions-of-access.pdf

This article may be used for research, teaching and private study purposes. Any substantial or systematic reproduction, re-distribution, re-selling, loan or sub-licensing, systematic supply or distribution in any form to anyone is expressly forbidden.

The publisher does not give any warranty express or implied or make any representation that the contents will be complete or accurate or up to date. The accuracy of any instructions, formulae and drug doses should be independently verified with primary sources. The publisher shall not be liable for any loss, actions, claims, proceedings, demand or costs or damages whatsoever or howsoever caused arising directly or indirectly in connection with or arising out of the use of this material.

Molecular Simulation
Vol. 37, No. 1, January 2011, 23–30

Taylor & Francis
Taylor & Francis Group

A molecular dynamics study of nano-bubble surface tension

H. Rezaei Nejad, M. Ghassemi*, S.M. Mirnouri Langroudi and A. Shahabi

Mechanical Engineering Department, K.N. Toosi University of Technology, Tehran, Iran

(*Received 31 January 2010; final version received 21 July 2010*)

The main purpose of this paper is to numerically investigate the effect of bubble curvature on the surface tension. The effect of surface wettability on the bubble shape is also investigated due to its direct effects on the bubble curvature. Also, the validity of Young–Laplace (Y–L) equation to describe the bubble characteristics in nano order is examined using the molecular dynamics (MD) simulations method. A computer code based on the MD method is developed. The code carries out a series of simulations to generate bubbles of various radii between two planar solid surfaces. In our simulation, the total volume of the simulation box as well as the surface wettability affects the bubble curvature. The pair potential for the liquid–liquid and liquid–solid interaction is considered using the Lennard-Jones model. Pressure tensor and density profile are locally calculated. Furthermore, liquid pressure is evaluated far from the interface using the virial theorem and gas pressure is obtained using an equation of state. It is observed that the gas pressure is almost independent of the bubble radius. However, the liquid pressure becomes more negative as the radius decreases. Surface tension is computed using the Y–L equation and compared with the surface tension directly computed from the MD simulation. The amount of surface tension increases with a decrease in the radius.

Keywords: molecular dynamics; bubble; surface tension; Young–Laplace; wettability

Downloaded At: 19:27 31 January 2011

1. Introduction

Vapour–liquid interfacial phenomena of micro-nano bubbles and droplets have recently attracted considerable attention of researchers in a wide range of fields. Researches in micro-nano bubbles and droplets dynamics and their physical properties gain an outstanding importance due to their statistical uncertainties in engineering and science fields [1–3], new methods of generating micro-nano bubbles [4] and their wide applications in the microelectromechanical systems (MEMS) technology and the biological remedy. Zhang et al. [5] have performed an experimental observation over nano-bubble nucleation where nano-bubbles of H_2 molecules are generated electrochemically in diluted sulphuric acid solution. However, experimental methods have not been able to completely study physical properties of nano bubbles and droplets because of their tiny size and delicateness. Due to obstacles in experimental methods, molecular dynamics (MD) simulation of such interfacial phenomena has drawn researchers' attention. In principle, any of gas, liquid, solid states and inter-phase phenomena can be simulated without the knowledge of thermo-physical properties such as thermal conductivity, viscosity, latent heat, saturation temperature and surface tension. In the droplet case several published papers have investigated the effect of curvature on the surface tension [6–9]. However, there is much less attention on the microscopic study of bubbles and their characteristics [10] due to their relative complexities of encountering higher densities, estimating the bubble centre and radius and investigating the uncertainties of the metastable liquid phase around the bubbles.

Additionally, implementing the macroscopic equation to nano-scale phenomena provides a lot of conveniences for researchers. However, using the macroscopic equation in nano order is still one of the most controversial issues. So, study of how far these macroscopic concepts are capable to describe microscopic phenomena is indeed important.

In the bubble case, as long as the size is of micrometer scale or larger, the Young–Laplace (Y–L) equation properly describes the bubble dynamics [11,12]. However, there is mistrust about using the Y–L equation for tiny bubbles, such as a 'nano-bubble'. A question arises when we try to explain the difference between inside and outside pressure of a bubble, because the pressure difference ($\Delta P = P_{\text{in}} - P_{\text{out}}$) extremely increases by decreasing the bubble radius. For instance, pressure difference of a bubble of radius 10 nm at room temperature ($\gamma \cong 0.073$ (N/m) for water) is 1.5×10^7 Pa or 150 atm [13]. It is a really high pressure that can mechanically make the bubble unstable. However, for a bulk bubble of radius 1 mm, the pressure difference is 146 Pa or 0.00146 atm. There are two points of view to describe this extreme difference. Firstly, Nagayama et al. [14] noted that the Y–L equation is no more applicable

*Corresponding author. Email: ghasemi@kntu.ac.ir

ISSN 0892-7022 print/ISSN 1029-0435 online
© 2011 Taylor & Francis
DOI: 10.1080/08927022.2010.513007
http://www.informaworld.com

for nano-order phenomena and an equation based on molecular level should be defined instead. The second point of view is that the Y–L equation is still applicable but the surface tension differs a lot from its bulk property.

The studies on droplets generally concluded that the surface tension decreases as the radius of the droplet decreases [6–9]. Nonetheless, recent investigations of nano-bubble surface tension with MD simulation gain unlike results. Park et al.'s. [15] reported that the surface tension of a micro-nano bubble rather increases slightly with a decrease in the bubble radius. In contrast, Matsumoto and Tanaka [13] noted that the vapour pressure and the surface tension do not depend on its curvature and they are in good agreement with the bulk properties of the bubble. As mentioned above, the treatment of surface tension in the case of bubble does not follow the previous studies in terms of the surface tension of the droplet.

The main concern of this paper is to study the effect of the bubble curvature on the surface tension. Also, the validity of the Y–L equation to describe the bubble characteristics in nano order is examined using the MD simulations method. A computer code based on the MD method is developed. The code carries out a series of simulations to generate bubbles of various radiuses between two planar solid surfaces. In our simulation, total volume of the simulation box as well as the surface wettability affects the bubble curvature.

2. Simulation method

The 3D view of the simulation box is depicted in Figure 1. As shown in Figure 1, the length, width and height of the simulation box size are $L_x = 43.2$ Å, $L_y = 49.8$ Å and $h = 46$ Å, respectively. In order to simulate bubble nucleation, we consider 1688 argon atoms (at its saturated liquid density) between two planar walls. Each wall

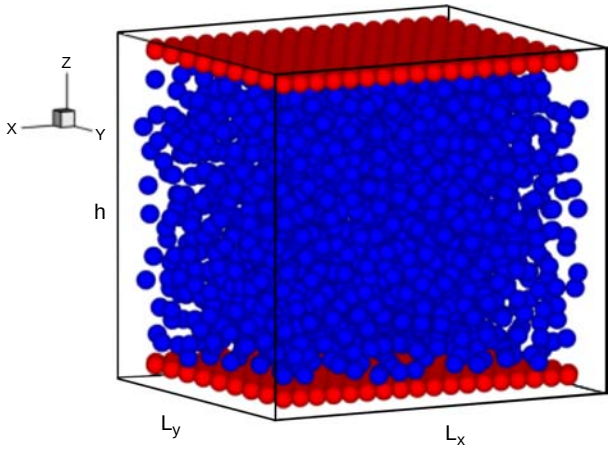

Figure 1. Simulation system for bubble formation and corresponding box size.

contains a layer of platinum atoms arranged as an face-centered cubic (FCC) lattice and its ‹111› face is in contact with liquid molecules [16]. Here, the lattice constant of platinum is 2.77 Å and the total number of platinum atoms is 648. A layer of phantom molecules is placed outside of each platinum surface. The well-known Lennard-Jones (L-J) pair potential is applied for the liquid–liquid interaction which is as follows:

$$U_{\mathrm{Ar-Ar}}(r_{ij}) = \varepsilon_{\mathrm{Ar}}\left(\left(\frac{\sigma_{\mathrm{Ar}}}{r_{ij}}\right)^{12} - \left(\frac{\sigma_{\mathrm{Ar}}}{r_{ij}}\right)^{6}\right), \qquad (1)$$

where in Equation (1), $r_{ij} = |\boldsymbol{r}_j - \boldsymbol{r}_i|$ denotes the magnitude of vector from atom j to atom i and ε and σ are L-J potential parameters; energy and length, respectively. The corresponding potential parameters of argon atoms are $\varepsilon_{\mathrm{Argon}} = 1.65 \times 10^{-21}$ J and $\sigma_{\mathrm{Argon}} = 3.4$ Å. Moreover, the potential among solid and liquid atoms is applied as below:

$$\begin{aligned} U_{\mathrm{Ar-Pt}}(r_{ij}) &= \varepsilon_{\mathrm{int}}\left(\left(\frac{\sigma_{\mathrm{int}}}{r_{ij}}\right)^{12} - \left(\frac{\sigma_{\mathrm{int}}}{r_{ij}}\right)^{6}\right) \\ &= \alpha\varepsilon_{\mathrm{Ar-Pt}}\left(\left(\frac{\sigma_{\mathrm{int}}}{r_{ij}}\right)^{12} - \left(\frac{\sigma_{\mathrm{int}}}{r_{ij}}\right)^{6}\right), \end{aligned} \qquad (2)$$

where $\varepsilon_{\mathrm{int}}$ is the wettability parameter and $\sigma_{\mathrm{int}} = (\sigma_{\mathrm{Argon}} + \sigma_{\mathrm{Platinum}})/2$ is the size parameter. The energy parameter $\varepsilon_{\mathrm{Ar-Pt}}$ is given by $\varepsilon_{\mathrm{Ar-Pt}} = (\varepsilon_{\mathrm{Argon}} \times \varepsilon_{\mathrm{Platinum}})^{1/2}$ based on the Lorentz–Berthelot combining rule [17,18]. The potential parameters for platinum are $\sigma_{\mathrm{Pt}} = 2.475$ Å and $\varepsilon_{\mathrm{Pt}} = 8.35 \times 10^{-20}$ J. Also, α is the potential energy factor indicating the strength of hydrophilic interaction [19].

Initially, the Noše–Hoover thermostat is applied to argon atoms in order to make the dimensionless liquid temperature $T = 0.8$. The temperature of platinum walls is adjusted by the phantom technique. The phantom molecules model the infinitely wide bulk solid kept at a constant temperature T with suitable heat conduction characteristics [20,21]. After initialisation, we switch off the Noše–Hoover thermostat, and the temperature of argon atoms is only regulated by solid walls temperature. In earlier MD works on bubble generation [13,14], external force was directly applied to liquid molecules that result in making a vacancy in liquid. This method of adding energy directly to the system seems too artificial. Hence, to make a more realistic situation, a different method is considered to simulate the bubble nucleation [22]. Here, external force is not directly applied to each molecule. Instead, the volume of the simulation box is increased which leads to a decrease in total density and pressure. Consequently, nucleation occurs as a result of metastable condition of liquid molecules. In the present study, to generate a bubble, the top wall is moved with the

Downloaded At: 19:27 31 January 2011

Table 1. Conditions and contact angle.

Label	ρ_{ave} (σ^{-3})	h (σ)	α_{bottom}	z_c (σ)	$r_b - 1$ (σ)	$r_b - 2$ (σ)	ρ_l (σ^{-3})	ρ_g (σ^{-3})	$\theta - 1$ (°)	$\theta - 2$ (°)
V1	0.631	14.37	0.0460	2.12	3.88	3.69	0.78	0.009	56.88	54.91
V2, E2	0.617	14.71	0.0460	2.40	4.34	4.15	0.79	0.008	56.35	54.71
V3	0.591	15.34	0.0460	2.63	4.89	4.85	0.81	0.004	56.56	57.15
V4	0.578	15.67	0.0460	2.75	5.09	5.00	0.82	0.006	57.29	56.63
V5	0.567	16.00	0.0460	2.85	5.34	5.11	0.82	0.001	57.71	56.09
V6	0.545	16.64	0.0460	2.97	5.61	5.43	0.83	0.003	58.07	56.83
E1	0.617	14.71	0.0375	1.52	4.85	4.70	0.81	0.002	71.63	71.12
E3	0.617	14.71	0.0545	2.94	4.11	3.99	0.79	0.017	44.29	42.66
E4	0.617	14.71	0.0630	3.40	4.06	4.09	0.79	0.008	31.76	33.81
E5	0.617	14.71	0.0716	3.94	3.93	3.82	0.79	0.011	–	–

velocity of $V_{top} = 1$ m/s to reach a specific height listed in Table 1. Moving the top wall results in changing liquid density and due to the metastable condition of the liquid [14], the bubble appears. Initially, several tiny unstable bubbles generated are scattered around the surface. After a proper long simulation time, they gather together and finally a large stable bubble generates [22]. After this step, the moving process is stopped and the simulation is prolonged for 200 ps to attain stable condition. Then, results are extracted through another 600 ps. It should be noted that we consider a quite wettable potential parameter ($\alpha = 0.0716$) on the top surface to prevent bubble nucleation on it, and change the wettability on the bottom surface as shown in Table 1. All simulations are performed with a time step of 5 fs. The cut-off radius of 4σ is selected. The equations of motion were integrated by the leap-frog Verlet algorithm. All quantities are non-dimensionalised according to σ, ε and m, which use the values of argon.

Downloaded At: 19:27 31 January 2011

3. Results and discussion

3.1 Density distribution and profile

As known, the bubble changes its position in the simulation box continuously which makes the bubble density profile and contour calculations a difficult task. To obtain the bubble position, we use a particle mesh scheme. In this method, at first, the centre of the voids in the simulation box is calculated by dividing the whole domain into small meshes (mesh size $= 1\sigma$). Then, the scheme looks for an assembly of vacant mesh. Then, the centre of the vacancy is calculated and the x and y positions of the centre of coordinate are adjusted to the centre of the vacancy. In the second step, at the centre of the vacancy, a thin plane in x–z direction with 1σ depth is considered [22]. A 2D mesh with 1σ grid size in x–z plane is generated and then the scheme applies a time average method in order to obtain the amount of density. A sliced view of the bubble is presented in Figure 2 in comparison with the density contour.

The volume of the simulation box depends on the time interval in which the top surface is moving. After reaching the stable condition, the simulation continues for 600 ps to extract the results. In this study, two possible effects on bubble curvature are considered. Case 1: in which the simulations are labelled as V1–V6, the effect of final simulation box volume (or final average density, ρ_{ave}) on the bubble radius, r_b, is investigated. Case 2: E1–E5, the effect of energy parameter of liquid–solid interaction potential ε_{int} (surface wettability) on the bubble curvature is studied (for a specific final average density).

In the first case, the 2D density distributions are shown in Figure 3 for V2, V4, V5 and V6. The first layer of Argon atoms is neglected in such a way that the shape of bubbles can be considered as part of a sphere. Also, it is shown that the radius of bubble increases as the volume increases which causes the liquid to expand and its pressure to decline. The hydrophilic interaction parameter between solid and liquid, α, for top wall and bottom wall is kept constant at 0.0716 and 0.046, respectively. Therefore, the contact angle between the bubble and the solid layer remains almost the same. The value of the contact angle is presented in Table 1.

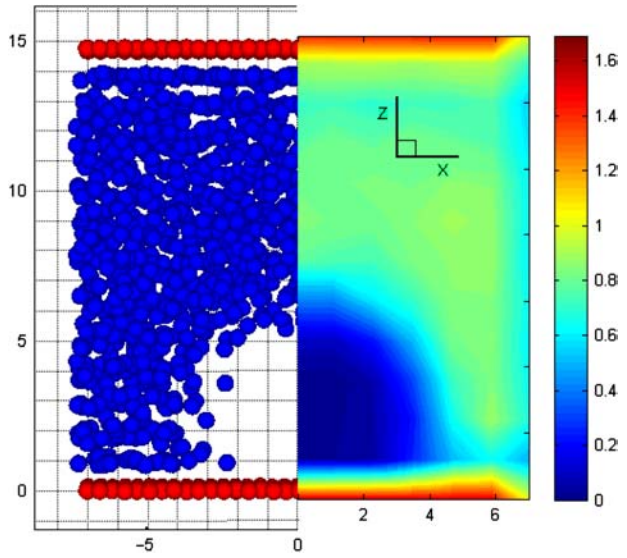

Figure 2. Sliced view of the simulation box in comparison with density contour.

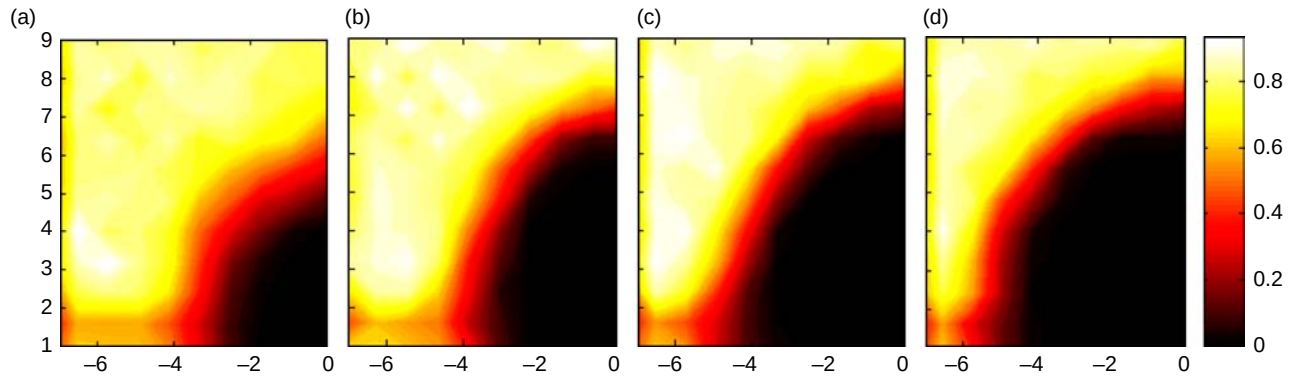

Figure 3. Density contours of the bubbles in x–z plane with the top wall $\alpha = 0.0716$ and the bottom wall $\alpha = 0.046$, corresponding values are listed in Table 1, (a) V2, (b) V4, (c) V5 and (d) V6.

In the second case, the effect of surface wettability on bubble curvature is predicted. Figure 4 depicts the density distribution of various wettabilities of the bottom wall while the upper wall wettability stays constant. It is obvious that the less wettable surface leads to more flattened shape. Furthermore, as wettability of the bottom surface increases, the contact angles from left to right decrease, see Figure 4 and Table 1. In Figure 4(e), as expected, the bubble is not generated on the down surface and is nucleated away from it because the wettability of the down surface is the most and the same as that of the top. It should be noted that in all simulations of the second case, the final volume of the simulation box (or ρ_{ave}) stays constant. Therefore, the wettability of the bottom surface is the only parameter that affects the shape of the bubble.

In order to calculate the contact angle and the surface tension, the centre of the bubble is determined by employing the least square fitting method to a chosen density contour line (all points on the line are at the same level). The amounts of this parameter, z_c, are given in Table 1. In E1–E5, when higher wettable solid surfaces are employed, more argon atoms are adsorbed by the solid and the bubble centre rises. Eventually, in E5, the bubble is completely separated from the surface ($z_c > r_{\text{b}}$).

By locating the bubble centre, the diagram of radial density distribution is obtained. To achieve this goal, we defined a spherical shell of inner radius r and outer radius $r + dr$ from the centre of the bubble. The radius increases from zero to the half length of the simulation box with $dr = 0.5\sigma$. Then, the average number of Argon atoms in each shell is calculated for the last 600 ps. The least square fitting of the tanh function well represents the numerical data. Figure 5 represents the radial density profiles with different ρ_{ave}. It is observed from the figure that the liquid density slightly decreases as r_{b} decreases. This implies that the liquid is on stretch that will be discussed in the following section.

The effect of bottom surface wettability on density profile is presented in Figure 6; it is noticed that by decreasing the surface wettability, the radius of the bubble increases; the details are presented in Table 1. Also, it can be seen that for E3–E5, the density profiles are almost the same, because the contact between the surface and the bubbles is weak, and the bubble is about to separate from the surface.

Two different approaches are used to calculate the radius of the bubble, r_{b}. In the first approach, since the centre of the bubble is calculated and the density of gas

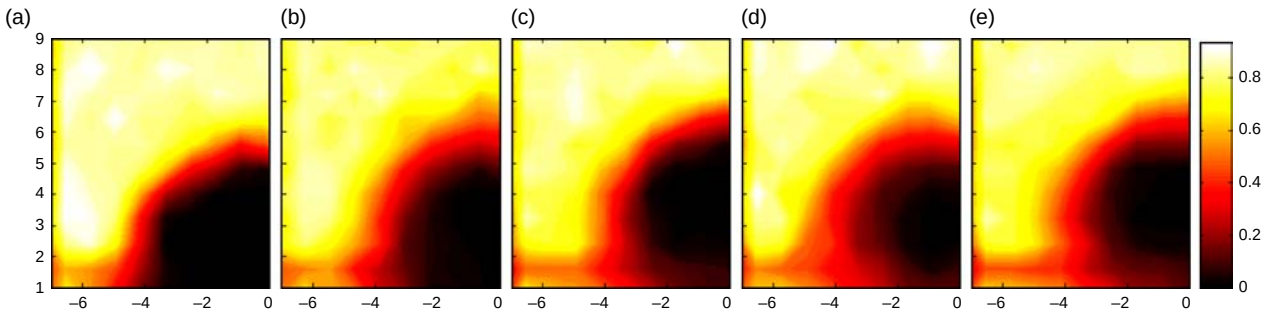

Figure 4. Density contours of the bubbles in x–z plane with the top wall $\alpha = 0.0716$ and the average density for all cases is $\rho_{\text{ave}} = 0.617$, also the bottom wall hydrophilic parameter α differs for each case, corresponding values are listed in Table 1, (a) E1, (b) E2, (c) E3, (d) E4 and (e) E5.

Downloaded At: 19:27 31 January 2011

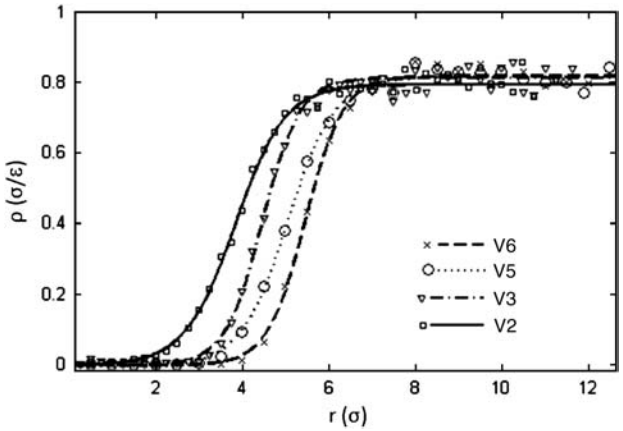

Figure 5. Radial density profiles for different final average densities, ρ_{ave}, of the simulation box.

and liquid is obtained from Figures 5 and 6, the radius of the bubble can be calculated according to Equation (3),

$$\rho_g v_g + \rho_l (v_{total} - v_g) = n, \tag{3}$$

where n denotes the total number of argon atoms, v_{total} is the volume of simulation box and v_g, the gas phase volume, is only a function of the r_b. Here, ρ_l and ρ_g are the liquid and gas densities, respectively. Since r_b is the only unknown parameter, it can be obtained using Equation (3). The bubble radius gained from this approach is presented in Table 1 by $r_b - 1$.

In the second approach, at first, surface tension, liquid pressure and gas pressure are calculated directly from the MD simulation which are illustrated in Sections 3.2 and 3.3. Considering the Y–L equation, Equation (9), the bubble radius, $r_b - 2$, can be obtained. The results are shown in Table 1.

Although the main purpose of this work is to investigate the effect of curvature on the surface tension, we have

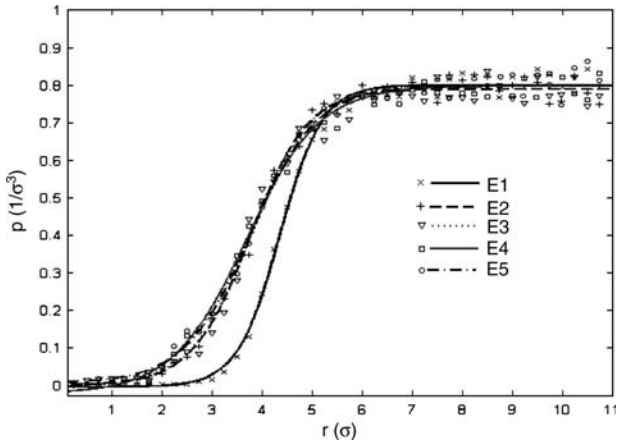

Figure 6. Radial density profiles for different bottom surface wettabilities, the parameter α for top surface is kept constant at 0.0716.

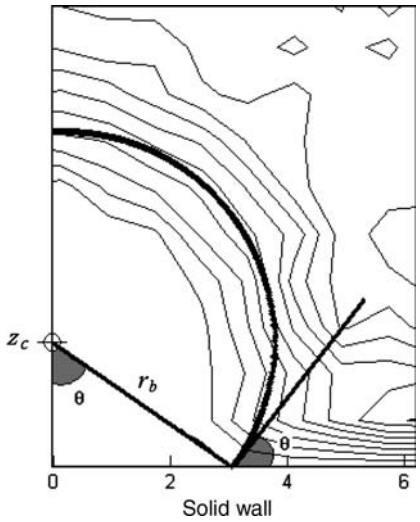

Figure 7. The description of the contact angle, z_c, θ, and r_b are the height of bubble centre, the contact angle and the bubble radius, respectively.

evaluated the contact angle for the sake of determining the effect of potential energy factor, α, on the shape of the bubble. To gain the contact angle, a circle with the radius obtained by Equation (3) and the centre of z_c, is fitted on density contour. Figure 7 illustrates the fitted circle for the case of E2. Here, solid wall locates at the height of zero. The contact angle θ is evaluated as $\cos(\theta) = z_c/r_b$. $\theta - 1$ and $\theta - 2$ are the bubble contact angles obtained by considering $r_b - 1$ and $r_b - 2$.

Table 1 summarises the results of the contact angle and all the required parameters to calculate it. In E1–E5, as α increases, the surface becomes more hydrophilic and absorbs more liquid atoms. So, the bubbles tend to separate from the surface and the contact angle obviously decreases. Also, in E5 there is no contact between the bubble and surface and z_c is bigger than r_b.

3.2 Pressure

In our MD simulations, it is necessary to calculate the pres-sure to monitor gas and liquid pressure as well as the pressure difference between bubble interior and exterior. The pressure is calculated using the following virial expression:

$$P = \frac{Nk_BT}{V} + \frac{1}{3V}\left\langle \sum_i^N r_i f_i \right\rangle. \tag{4}$$

In the special case of pair-potential simulation, the virial equation is usually written in a pairwise manner [23].

$$P = \frac{Nk_BT}{V} + \frac{1}{6V}\left\langle \sum_i^N \sum_{j\neq i}^N r_{ij} f_{ij} \right\rangle, \tag{5}$$

Downloaded At: 19:27 31 January 2011

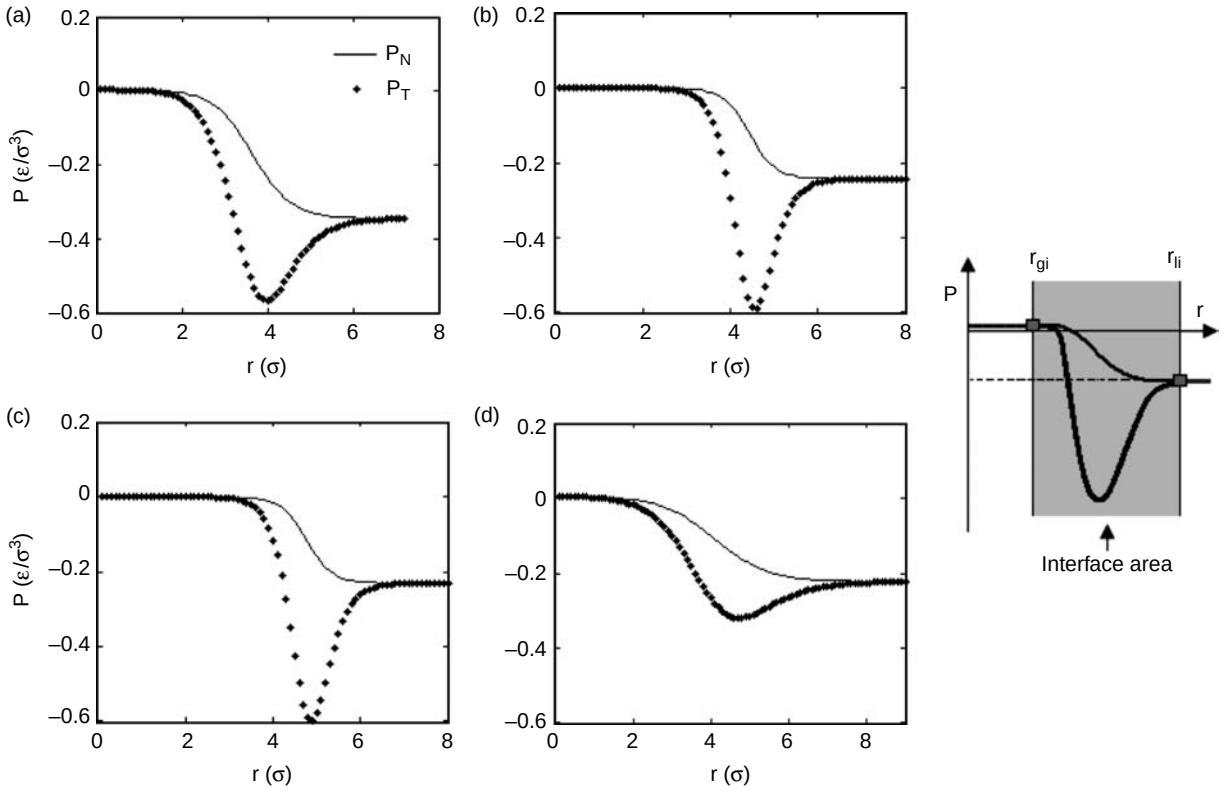

Figure 8. Radial distribution of pressure and schematic view including important points (r_{li} and r_{gi}): (a) V2, (b) V3, (c) V4 and (d) V5.

where V, T and N are the volume, temperature and the number of atoms of calculation domain, respectively. f_{ij} is the force on atom i due to atom j, $r_{ij} = r_j - r_i$ and k_B is Boltzmann's constant.

To estimate the pressure profile, we defined a spherical shell of inner radius r and outer radius $r + dr$ from the centre of bubble, as in Section 3.1. The pressure of each shell is computed by the virial equation and the amount of pressure is assigned to the radius of the shell. Figure 8 shows the pressure profiles in radial coordinate.

P_g and P_l denote the gas pressure and the liquid pressure, respectively. Liquid pressure is computed by averaging the amount of pressure from Equation (5) far from the liquid–gas interface. Equation (5) is not appropriate to calculate the gas pressure due to low number of argon atoms inside the bubble and poor statistics. Hence, a separate MD simulation for the vapour phase is carried out to obtain an equation of state (the relation between ρ_g and P_g at given T). P_g is calculated by evaluating the density inside the bubble and considering the equation of state. All the calculated pressures are presented in Table 2.

In order to calculate the surface tension of the bubble directly from the MD simulation, local pressure is required. The pressure tensor for the spherical bubble is written as

$$P(r) = P_N(r)[e_r e_r] + P_T(r)[e_\theta e_\theta + e_\phi e_\phi], \qquad (6)$$

where e_r, e_θ and e_ϕ are orthogonal unit vectors and $P_N(r)$ and $P_T(r)$ are the normal and transverse components of pressure tensor which are functions of r from the centre of bubble only. The general condition of mechanical equilibrium, $\nabla \cdot P = 0$, leads to

$$P_T(r) = P_N(r) + \frac{r}{2}\frac{dP_N(R)}{dr}. \qquad (7)$$

Here, $P_N(r)$ can be written as follows:

$$P_N(r) = P_K(r) + P_U(r), \qquad (8)$$

Table 2. Survey of measured values and surface tension.

			γ (ε/σ²)	
Label	P_l (ε/σ³)	P_g (ε/σ³)	Y–L	MD
V1	−0.363	0.0063	0.7164	0.6810
V2, E2	−0.317	0.0056	0.7000	0.6700
V3	−0.229	0.0028	0.5668	0.5620
V4	−0.217	0.0042	0.5630	0.5530
V5	−0.197	0.0007	0.5279	0.5050
V6	−0.195	0.0021	0.5529	0.5350
E1	−0.260	0.0014	0.6339	0.6140
E3	−0.324	0.0120	0.6905	0.6716
E4	−0.337	0.0056	0.6955	0.7010
E5	−0.338	0.0078	0.6795	0.6602

Downloaded At: 19:27 31 January 2011

Downloaded At: 19:27 31 January 2011

where $P_K(r) = k_B T\rho(r)$. In order to calculate $P_U(r)$, we have followed the method that Thompson and Gubbins [24] proposed in their paper.

The calculated local, normal and transverse pressures in cases V2–V5 are depicted in Figure 8. Specified coloured region is defined as the vapour–liquid interface, see Figure 8. r_{gi} is the beginning of the interface region and r_{li} is the end of it. To better verify this point, one can use the density profile. It is observed from the density profile that the densities at r_{gi} and r_{li} are almost equal to gas- and liquid-phase densities, respectively. So, the region between these two points is assumed as vapour–liquid interface. In this region, the pressure profile has an intensive variation. There is no reason for the existence of such an intensive change in the pressure profile except the effect of surface tension.

Figure 9 shows the dependence of gas and liquid pressure on r_b As shown, it is observed that P_g is almost independent of r_b. However, P_l slightly increases as the radius increases. With an increase in r_b, the liquid is in less stretch which results in less negative pressure values. It is observed that the pressure difference between liquid and gas is really high and much bigger than the bulk value.

3.3 *Surface tension*

As it is mentioned in Section 1, using the Y–L equation in nano order is suspect due to the extreme atmospheric pressure difference gained from the Y–L equation. Our results in Section 3.2 which are directly computed from MD simulation, however, confirm that there is a high-pressure difference between inside and outside of the bubble. For instance, in the case V1 ($\Delta P = P_g - P_l = 155$ atm). Thus, we conclude that the high-pressure difference exists because of the nature of nano bubbles and it is not caused by employing the Y–L equation.

In the present study, we apply the Y–L equation in order to calculate the surface tension. The difference between the liquid and gas pressure far from the interface, P_l and P_g, is used in the Y–L equation to calculate the surface tensions. The Y–L equation for a spherical-shaped bubble or droplet is readily deduced from stability theory,

$$P_{in} = P_{out} + \frac{2\gamma}{r_b}, \tag{9}$$

where P_{in}, P_{out} and γ denote the interior and exterior bubble (droplet) pressure and surface tension, respectively.

In order to check the validity of the Y–L equation in nano order, the surface tension is directly computed from the MD simulation, as well. Surface tension can be computed as

$$\gamma^3 = -\frac{1}{8}(P_l - P_g)^2 \int_0^\infty r^3 \frac{dP_N(r)}{dr} dr, \tag{10}$$

where P_l and P_g are liquid and gas pressures far from the interface. $dP_N(r)/dr$ is gained from differentiating Equation (8).

The treatment of bubble surface tension with respect to bubble radius is shown in Figure 10 from both the Y–L equation and direct MD simulation. The result at $r_b \to \infty$ is directly obtained from a separate MD simulation of a flat surface [25]. It is observed that the surface tensions computed from the Y–L equation and direct MD simulations are in good agreement and show the same trend. As shown, the surface tension slightly increases as the bubble radius decreases. Also, with an increase in bubble radius, surface tension tends to the bulk value ($\gamma_\infty = 0.561$).

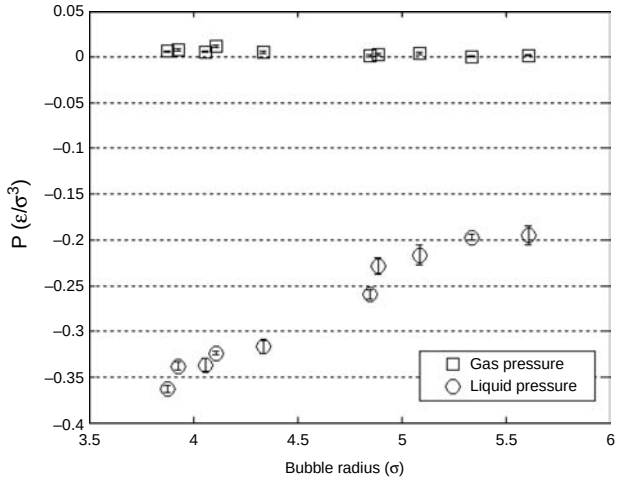

Figure 9. Pressure of gas and liquid with respect to the bubble radius, r_b. The error bars show the standard deviation (SD), which is estimated by dividing the total simulation run of 600 ps into three parts of 200 ps. Typical SD is 0.0009 for gas and 0.006 for liquid.

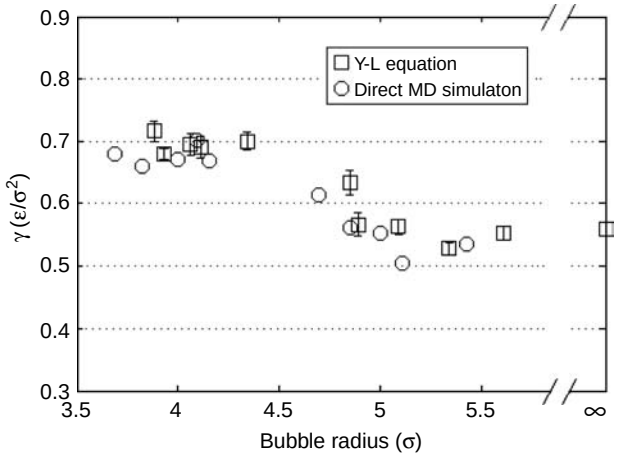

Figure 10. Variation of surface tension with respect to r_b. The error bars of the surface tension obtained from the Y–L equation are the result of P_l and P_g. The surface tension gained from direct MD simulation is calculated through the total simulation run of 600 ps.

This is in accordance with Park et al.'s [15] study that concluded that the surface tension of a nano bubble slightly increases from the bulk values (up to 15%) when bubble radius decreases. Park et al. used local pressure tensor to obtain surface tension. On the other hand, Matsumoto and Tanaka [13] calculated the surface tension of a nano bubble from the Y–L equation and noted that it is independent of the radius. This contradiction may arise from the difference between the radiuses of simulated bubbles where Matsumoto and Tanaka's study of surface tension only covers the bubbles with the radiuses more than 5σ. As they mentioned, they tried to generate tinier bubbles but failed. However, Park's and our results predicted the surface tension of tinier bubbles. More details about surface tension for both cases V1–V6 and E1–E5 are given in Table 2.

4. Conclusions

In this study, the bubble nucleation is investigated using a series of MD simulations. The effect of surface wettability and ρ_{ave} on bubble shape and contact angle is predicted. In addition, the dependence of surface tension on bubble radius is studied from both the direct MD simulation and the Y–L equation. The validity of the Y–L equation to describe the bubble characteristics in nano order is examined using direct MD simulations. In order to calculate the surface tension from the Y–L equation, the gas pressure is evaluated using the equation of state obtained from a separate MD simulation. The liquid pressure is evaluated, employing the virial theorem far from the interface. Main results are listed as follows:

- It is found that less wettable surface leads to more flattened bubble shape and greater contact angle. Also, the contact angle does not change for various bubble radiuses, when surface wettability remains constant.
- It is shown that the gas pressure is almost independent of the bubble radius. However, the liquid pressure increases with an increase in the bubble radius.
- The surface tension slightly increases as the radius decreases. Additionally, with an increase in the bubble radius the surface tension tends to the bulk value.
- In the present study, both the gas and liquid phases are made of the same material, argon atoms. In such a case, our simulation result of extreme pressure difference between the gas and liquid phases suggests that nano bubble nucleation is only possible in highly stretched liquid. Since this pressure deference is directly calculated from MD simulation, it does not contradict the validity of using the Y–L equation in nano scale.
- The bubble radius, the contact angle and especially the surface tension gained from both the Y–L equation and direct MD simulation present the same trend and the results match each other well .

Downloaded At: 19:27 31 January 2011

References

[1] J.S. Rowlinson and B. Widom, *Molecular Theory of Capillarity*, Oxford University Press, New York, 1982.

[2] J. Israelachvili, *Intermolecular and Surface Forces*, Academic Press, San Diego, CA, 1992.

[3] J.G. Weng, S.H. Park, and C.L. Tien, *Interfacial ambiguities in microdroplets and microbubbles*, Microscale Thermophys. Eng. 4 (2000), pp. 83–87.

[4] M. Takahashi, T. Kawamura, Y. Yamamoto, H. Ohnari, S. Himuro, and H. Shakkutsui, *Effect of shrinking microbubble on gas hydrate formation*, J. Phys. Chem. C 107 (2003), pp. 2171–2173.

[5] L. Zhang, Y. Zhang, X. Zhang, Z. Li, G. Shen, M. Ye, C. Fan, H. Fang, and J. Hu, *Electrochemically controlled formation and growth of hydrogen nanobubbles*, Langmuir 22 (2006), pp. 8109–8113.

[6] S.M. Thompson, K.E. Gubbins, J.P.R.B. Walton, R.A.R. Chantry, and J.S. Rowlinson, *A molecular-dynamics study of liquid-drops*, J. Chem. Phys. 81 (1984), pp. 530–542.

[7] R.C. Tolman, *The effect of droplet size on surface tension*, J. Chem. Phys. 17 (1949), pp. 333–337.

[8] H. Yaguchi, T. Yano, and S. Fujikawa, *Molecular dynamics study of evaporation of nanodroplets*, Proceedings of the International Conference on Multiphase Flow, Liepzig (2007)

[9] K. Koga, X.C. Zeng, and A.K. Shchekin, *Validity of Tolman's equation: How large should a droplet be?* J. Chem. Phys. 109 (1998), pp. 4063–4070.

[10] S. Maruyama, *Molecular dynamics method for microscale heat transfer*, in *Advances in Numerical Heat Transfer*, W.J. Minkowycz, and E.M. Sparrow, eds., Taylor & Francis, New York, 2000, pp. 189–226.

[11] C.E. Brennen, *Cavitation and Bubble Dynamics*, Oxford University Press, Oxford, 1995.

[12] V.P. Skripov, *Metastable Liquids*, Wiley, New York, 1974.

[13] M. Matsumoto and K. Tanaka, *Nano bubble-size dependence of surface tension and inside pressure*, Fluid Dyn. Res. 40 (2008), pp. 546–553.

[14] G. Nagayama, T. Tsuruta, and P. Cheng, *Molecular dynamics simulation on bubble formation in a nanochannel*, Int. J. Heat Mass Transfer 49 (2006), pp. 4437–4443.

[15] S.H. Park, J.G. Weng, and C.L. Tien, *A molecular dynamics study on surface tension of microbubbles*, Int. J. Heat Mass Transfer 44 (2001), pp. 1849–1856.

[16] T. Kimura and S. Maruyama, *Molecular dynamics simulation of heterogeneous nucleation of a liquid droplet on a solid surface*, Microscale Thermophys. Eng. 6 (2002), pp. 3–13.

[17] E.M. Yezdimer, A.A. Chialvo, and P.T. Cummings, *Examination of chain length effects on the solubility of alkenes in near-critical and supercritical aqueous solutions*, J. Phys. Chem. B 105 (2001), pp. 841–847.

[18] J. Delhommelle and P. Millie, *Inadequacy of the Lorentz–Berthelot combining rules for accurate predictions of equilibrium properties by molecular simulation*, Mol. Phys. 99 (2001), pp. 619–625.

[19] G. Nagayama and P. Cheng, *Effects of interface wettability on microscale flow by molecular dynamics simulation*, Int. J. Heat Mass Transfer 47 (2004), pp. 501–513.

[20] J.C. Tully, *Dynamics of gas–surface interactions: 3D generalized Langevin model applied to fcc and bcc surfaces*, J. Chem. Phys. 73 (1980), pp. 1975–1985.

[21] J. Blömer and A.E. Beylich, *MD-simulation of inelastic molecular collisions with condensed matter surfaces*, Proceedings of the 20th International Symposium on Rarefied Gas Dynamics, Beijing (1997)

[22] S. Maruyama and T. Kimura, *A molecular dynamics simulation of a bubble nucleation on solid surface*, ASME/JSME Thermal Engineering Joint Conference, San Diego, CA (1999)

[23] T. Ikeshoji, B. Hafskjold, and H. Furuholt, *Molecular-level calculation scheme for pressure in inhomogeneous systems of flat and spherical layers*, Mol. Simulat. 29 (2003), pp. 101–109.

[24] S.M. Thompson and K.E. Gubbins, *A molecular dynamics study of liquid drops*, J. Chem. Phys. 81 (1984), pp. 530–542.

[25] J.S. Rowlinson and B. Widom, *Molecular Theory of Capillarity*, Clarendon Press, Alderley, 1982.